



Cite this: *Phys. Chem. Chem. Phys.*,
2022, **24**, 25853

nablaDFT: Large-Scale Conformational Energy and Hamiltonian Prediction benchmark and dataset

Kuzma Khrabrov,^{id}*^a Ilya Shenbin,^{id}^c Alexander Ryabov,^{id}^{de} Artem Tsypin,^{id}^a
 Alexander Telepov,^{id}^a Anton Alekseev,^{id}^{cg} Alexander Grishin,^{id}^a
 Pavel Strashnov,^{id}^a Petr Zhilyaev,^d Sergey Nikolenko^{id}^{cf} and Artur Kadurin^{id}*^{ab}

Electronic wave function calculation is a fundamental task of computational quantum chemistry. Knowledge of the wave function parameters allows one to compute physical and chemical properties of molecules and materials. Unfortunately, it is infeasible to compute the wave functions analytically even for simple molecules. Classical quantum chemistry approaches such as the Hartree–Fock method or density functional theory (DFT) allow to compute an approximation of the wave function but are very computationally expensive. One way to lower the computational complexity is to use machine learning models that can provide sufficiently good approximations at a much lower computational cost. In this work we: (1) introduce a new curated large-scale dataset of electron structures of drug-like molecules, (2) establish a novel benchmark for the estimation of molecular properties in the multi-molecule setting, and (3) evaluate a wide range of methods with this benchmark. We show that the accuracy of recently developed machine learning models deteriorates significantly when switching from the single-molecule to the multi-molecule setting. We also show that these models lack generalization over different chemistry classes. In addition, we provide experimental evidence that larger datasets lead to better ML models in the field of quantum chemistry.

Received 26th August 2022,
Accepted 12th October 2022

DOI: 10.1039/d2cp03966d

rsc.li/pccp

1 Introduction

The solution of the many-particle Schrödinger equation (SE) for electrons makes it possible to describe matter at the level of chemical bonds for molecules and band structure for crystals. In turn, the electronic system of matter determines a large number of its equilibrium and transport properties, which opens up vast opportunities in the search for new molecules such as prospective drugs or catalysts and new materials such as novel superhard, superconducting, low-dimensional, and other materials.

Solving the many-particle SE is a complex task that has attracted a lot of attention from several generations of

researchers, but, unfortunately, its analytical solution is still unknown. However, there exist a wide variety of numerical methods that solve it on different levels of precision. These methods comprise a hierarchy that trades off accuracy against computational cost and the number of electrons whose motion one can calculate in reasonable time using a particular technique.

At the top of the hierarchical pyramid are two families of Post-Hartree–Fock¹ and quantum Monte Carlo methods.² They are very accurate (approximately 1 kcal mol^{−1}) but computationally expensive, allowing to consider systems of up to tens of electrons. All of them are based on manipulating the many-body wave function, which is represented as an expansion of one-electron orbitals with adjustable coefficients. Optimization search is performed in the space of these adjustable coefficients to find a multi-particle wave function that provides the minimum energy of the system. Therefore, it most closely corresponds to the “real” multi-particle wave function of the ground state (the minimum energy state).

The second step of the hierarchical pyramid is taken by the density functional theory (DFT) method,^{3–5} which is currently the primary approach for solving the many-particle SE for electrons.

DFT is a mean-field method, where the many-particle problem is divided into several single-particle problems, and one solves SE

^a AIRI, Kutuzovskiy prospect house 32 building K.1, Moscow, 121170, Russia.
E-mail: kadurin@airi.net, khrabrov@airi.net

^b Kuban State University, Stavropolskaya Street, 149, Krasnodar 350040, Russia

^c St. Petersburg Department of Steklov Mathematical Institute of Russian Academy of Sciences, nab. r. Fontanki 27, St. Petersburg 191011, Russia

^d Center for Materials Technologies, Skolkovo Institute of Science and Technology, Bolshoy Boulevard 30, bld. 1, Moscow, 121205, Russia

^e Moscow Institute of Physics and Technology (National Research University), Institutskiy lane, 9, Dolgoprudny, Moscow Region 141700, Russia

^f ISP RAS Research Center for Trusted Artificial Intelligence, Alexander Solzhenitsyn st. 25, Moscow, 109004, Russia

^g St. Petersburg University, 7-9 Universitetskaya Embankment, St Petersburg, 199034, Russia

for a single electron in the effective field of other electrons. The main difference between this method and more accurate ones is that it manipulates not the many-particle wave function but electron density, which is an observable quantity. DFT makes it possible to consider systems on a scale of 1000 electrons⁶ with satisfactory accuracy (approximately 10 kcal mol⁻¹), thus scaling up to systems that are already nano-objects such as nanotubes and fullers, pieces of proteins, or parts of catalytic surfaces. Accuracy of the DFT is determined by the so-called exchange-correlation (XC) functional,⁷⁻⁹ which again has an accuracy/complexity tradeoff hierarchy within itself. It is believed that by looking for a fast and accurate exchange-correlation functional it may be possible to improve DFT's accuracy up to 1 kcal mol⁻¹, thus making it almost equal in accuracy to the methods at the very top.

On the nominal third step of the hierarchy are the so-called parametric methods such as the tight-binding method,¹⁰ which require a parameterization of the Hamiltonian. They make calculations possible for extensive systems up to a tens of thousand electrons.¹¹ However, the non-deterministic pre-parameterization step and large volatility in the resulting accuracy make this method less popular than DFT.

In addition to traditional numerical methods for solving the many-body SE for electrons, machine learning (ML) methods have emerged in abundance, looking for their own place in the hierarchy of accuracy/complexity. One promising direction to incorporate ML into the field is to develop a family of trial wave functions based on deep neural networks (NN); recent results show that it can outperform the best highly accurate quantum Monte-Carlo methods.^{12,13} Another direction is to directly predict the wave-function, electron densities, and/or the Hamiltonian matrix from atom coordinates (system configuration).¹⁴⁻¹⁸ The third direction is to use neural networks to model the XC functional for high accuracy DFT.¹⁹⁻²⁶

The general framework of *ab initio* molecular property prediction consists of two steps: first compute the electron structure of a specific molecular conformation or a set of conformations, and then calculate desired properties based on the results of the first step. The second step is relatively

simple, but total computational complexity could be too high depending on the method used on the first step.

One straightforward approach to avoid this complexity is to train a machine learning model to predict desired molecular properties directly, shortcutting around the electron structure part. However, this approach may lack generalization since one would need to develop and train a separate new model for each new property.

Recent studies have shown promising results in the field of electron structure prediction using a number of different ML methods. It avoids costly computations of DFT (or higher order) methods by substituting it with a relatively simple ML model but keeping the generalized property computation framework. In this way, the method only needs a single ML model for all necessary properties (Fig. 1).

Though there exist recent advances in Hamiltonian matrix approximation using ML (see Section 2), these studies suffer from two serious drawbacks. First, all models were trained and tested in the single-molecule setup (both training and testing on different conformations of the same molecule), and all models have problems with scaling up to larger molecular structures. In our study we focus on exploring these drawbacks.

An important inspiration for this work comes from the lack of datasets that could be used to train such models. The expressive power of machine learning models is meaningless unless supported by the size and variability of training data. Related fields are seeing the rise of large-scale datasets of small molecules and compounds where the necessary properties have been established by accurate and computationally expensive methods; for example, t6 he MOSES benchmarking platform²⁷ has compared molecular generation models for drug discovery based on a subset of the ZINC clean leads dataset.²⁸ Other examples of large-scale datasets with results of DFT calculations are *Open Catalyst 2020 (OC20)* and *2022 (OC22)*.^{29,30} These datasets together contain 1.3 million molecular relaxations with results from over 260 million DFT calculations.

Large-scale datasets have allowed to achieve impressive results in the field of Natural Language Processing. One of the key reasons of the success of the Transformer-based



Fig. 1 Possible approaches to *ab initio* molecular property prediction.

models,³¹ such as BERT³² or GPT-3,³³ was the access to a huge training corpus. It has been shown in the domain of medicinal chemistry³⁴ that degradation in the accuracy from the full dictionary to a 30% of the dictionary is significant for disease linking in clinical trials. Apart from the quality increase, bigger and more diverse datasets are important for models robustness. Work of Tutubalina *et al.*³⁵ elaborates that the generalization ability of machine learning models is influenced by whether the test entity/relation has been presented in the training set.

In this work, we introduce a new large-scale dataset that contains structures and Hamiltonian matrices for about million conformations of about 6 million conformations of about 1 million molecular structures, with electronic properties computed with the Kohn–Sham method. This dataset allows for comparisons between DFT-based models in different settings, in particular generalization tests where the training and test sets contain different molecules. In the way of benchmarking, we adapt several classical and state of the art DFT-based models and compare their results on our dataset, drawing important conclusions about their expressivity, generalization power, and sensitivity to data size and training regimes. The models considered in this work come in two varieties, either estimating the potential energy estimation or predicting the Hamiltonian coefficients.

The paper is organized as follows. Section 2 describes related prior art, including datasets and methods as well as modern AI applications. Section 3 introduces the terminology used throughout this paper and sets up the mathematical foundations. Section 4 describes our new dataset, and Section 5 introduces the models used in our benchmark. Section 6 shows benchmark setup and results and discusses the outcomes of our experimental study, and Section 7 concludes the paper.

2 Related work

DFT allows to predict the behaviour of complex systems of atoms (molecules, materials) *ab initio*, based directly on quantum mechanics. However, accurate quantum-chemical computations have prohibitive computational costs. One possible solution is to use sufficiently simple analytic approximations to overly complex functions such as the total energy of the system.³⁶ Another approach, which has been rapidly gaining prominence over the last decade, is to learn such approximations in the form of various machine learning models.

2.1 Datasets

Several datasets with DFT calculations have been released.

The Quantum Machines 9 (QM9) dataset presents molecular structures and properties obtained from quantum chemistry calculations for the first 133 885 molecules of the chemical universe GDB-17 database.³⁷ The dataset corresponds to the GDB-9 subset of all neutral molecules with up to nine heavy atoms (CONF), not counting hydrogen. Additionally, the dataset

includes 6095 constitutional isomers of C₇H₁₀O₂. For all molecules, calculated parameters include equilibrium geometries, frontier orbital eigenvalues, dipole moments, harmonic frequencies, polarizabilities, and thermochemical energetics corresponding to atomization energies, enthalpies, and entropies at ambient temperature. These properties have been obtained at the B3LYP/6-31G(2df,p) level of theory. For a subset of 6095 constitutional isomers, these parameters were calculated at the more accurate G4MP2 level of theory.

Along with their Accurate Neural network engINe for Molecular Energies (ANAKIN-ME, or ANI), Smith *et al.*³⁸ released ANI-1,³⁹ a dataset of non-equilibrium DFT total energy calculations for organic molecules that contains \approx 20m molecular conformations for 57 462 molecules from the GDB-11 database.^{40,41} Atomic species are limited to C,N,O atoms (with hydrogens added separately with RDKit), and the number of heavy atoms varies from 1 to 8. All electronic structure calculations in the ANI-1 dataset are carried out with the ω B97x⁴² density functional and the 6-31 G(d) basis set in the Gaussian 09 electronic structure package.

Quantum-Mechanical Properties of Drug-like Molecules (QMugs) is a data collection of over 665k curated molecular structures extracted from the ChEMBL database.⁴³ Three conformers per compound were generated, and the corresponding geometries were optimized using the GFN2-xTB method,⁴⁴⁻⁴⁶ with a comprehensive array of quantum properties computed at the DFT level of theory using the ω B97X-D functional⁴⁷ and the def2-SVP Karlsruhe basis set.⁴⁸

2.2 Methods and applications

The field was opened by Snyder *et al.*⁴⁹ who used traditional machine learning models to approximate density functionals in Kohn–Sham DFT for a small number of fermions (up to 4 electrons). The *SchNet* model by Schütt *et al.*¹⁵ introduced a deep neural network approach to physical chemistry problems, specifically to the prediction of molecular conformation energy. This served as a starting point for a plethora of publications addressing different tasks in the field. Hermann *et al.*⁵⁰ and Pfau *et al.*⁵¹ proposed *PauliNet* and *Ferminet* respectively, two different deep learning wave function ansatzes that achieve nearly exact solutions of the electronic Schrödinger equation for single atoms or small molecules such as LiH, ethanol, or bicyclobutane. Gao and Günnemann⁵² PESNet outperformed previous works in terms of computational cost while matching or surpassing their accuracy. However, these approaches are very hard to scale both with the size of the molecular system and with the number of molecules. As reported by Gao and Günnemann,⁵² it takes 854, 4196, and 89 hours of training on an NVidia A100 GPU for *PauliNet*, *Ferminet*, and *PESNet* respectively for a system of only two nitrogen atoms, so further research is needed to make this approach scalable.

Advances in the field of AI for fundamental problem solving have shown promising results in a series of domains. In particular, Eremin *et al.*⁵³ recently designed, synthesized and tested a novel quasicrystal with the help of state-of-the-art machine learning models. Yakubovich *et al.*⁵⁴ used deep

generative models to search for molecules suitable for triplet-triplet fusion with potential applications in blue OLED devices, finding significantly increased performance in terms of generated lead quality. Wan *et al.*⁵⁵ applied a hybrid DFT-ML approach to study catalytic activity of materials. Schleder *et al.*⁵⁶ used machine learning techniques and DFT to identify thermodynamically stable 2D materials. Recently, Ritt *et al.*⁵⁷ elucidated key mechanisms for ion selectivity in nanoporous polymeric membranes by combining first-principles simulations with machine learning. Janet *et al.*⁵⁸ developed a ML-based approach for accelerated discovery of transition-metal complexes which allows to evaluate a large chemical compound space in a matter of minutes. Ye *et al.*⁵⁹ reviewed recent advances in applying DFT in molecular modeling studies of COVID-19 pharmaceuticals.

2.3 Importance

Mata and Suhm⁶⁰ pointed out the importance of benchmarking for computational quantum chemistry methods. Following them, we believe that it is crucial to establish a reliable and comprehensive benchmark procedure for machine learning methods in quantum chemistry. A transparent and reproducible assessment of accuracy and generalization power for novel ML approaches represents an important stepping stone towards future successes in many applied fields of quantum chemistry.

3 Theoretical foundations

3.1 Conformations

Conformations are structural arrangements of the same molecule that differ by rotation around single bonds and bond stretching. In molecular modeling, conformational analysis is a crucial step because it helps to cut down the time spent screening compounds for activity. For example, most drugs are flexible molecules that can take on various conformations, so conformations are crucial in the prediction of a drug's biological activity as well as its physico-chemical characteristics. Conformational analysis is related to the investigation of the total energies of different conformations for a given molecule (conformational energies). These energies represent important chemical properties that require benchmarking of various DFT methods.

3.2 DFT

Anti-symmetrized products of single-electron functions or molecular orbitals are frequently used in quantum chemistry to express the electronic wave function Ψ associated with the electronic time-independent Schrödinger equation

$$\hat{H}\Psi = E\Psi,$$

These single-particle functions are usually defined in a local atomic orbital basis of spherical atomic functions $|\psi_m\rangle = \sum_i c_m^i |\phi_i\rangle$, where $|\phi_i\rangle$ are the basis functions and c_m^i are the coefficients. As a result, one can represent the electronic Schrödinger equation in matrix form as

$$\mathbf{F}_\sigma \mathbf{c}_\sigma = \epsilon_\sigma \mathbf{S} \mathbf{c}_\sigma,$$

where \mathbf{F} is the Fock matrix (otherwise called the Hamiltonian matrix \mathbf{H}):

$$\mathbf{H}_{ij} = \langle \phi_i | \hat{H} | \phi_j \rangle,$$

\mathbf{S} is the overlap matrix:

$$S_{ij} = \langle \phi_i | \phi_j \rangle,$$

\mathbf{c} is the vector of coefficients, and σ is the spin index.

In matrix form, the single-particle wave function expansion can be represented by using Einstein summation as

$$\psi_i^\sigma(\vec{r}_1) = C_{\mu i}^\sigma \phi_\mu(\vec{r}_1).$$

Therefore, the density matrix is represented as

$$D_{ij}^\sigma = C_{ik}^\sigma C_{jk}^\sigma$$

In DFT, the matrix \mathbf{F} corresponds to the Kohn–Sham matrix:

$$F_{ij}^\sigma = Hc_{ij}^\sigma + J_{ij}^\sigma + V_{ij}^{\text{xc}}$$

where Hc_{ij}^σ is the core Hamiltonian matrix, J_{ij}^σ is the Coulomb matrix, and V_{ij}^{xc} is the exchange-correlation potential matrix.

In DFT, the total energy of the system (*e.g.*, total energy of a conformation) can be expressed as

$$E_{\text{total}} = D_{ij}^T (T_{ij} + V_{ij}) + \frac{1}{2} D_{ij}^T D_{\lambda\beta}^T (ij|\lambda\beta) + E_{\text{xc}}[\rho_\alpha, \rho_\beta],$$

where T is the noninteracting quasiparticle kinetic energy operator, V is the nucleus-electron attraction potential, D is the total electron density matrix, and E_{xc} is the (potentially nonlocal) exchange, correlation, and residual kinetic energy functional. The residual kinetic energy term is usually quite small and is often incorporated in correlation term of E_{xc} .

One can represent the Hamiltonian matrix in block form:¹⁶

$$\mathbf{H} = \begin{bmatrix} \mathbf{H}_{11} & \cdots & \mathbf{H}_{1j} & \cdots & \mathbf{H}_{1n} \\ \vdots & \ddots & \vdots & & \vdots \\ \mathbf{H}_{i1} & \cdots & \mathbf{H}_{ij} & \cdots & \mathbf{H}_{in} \\ \vdots & & \vdots & \ddots & \vdots \\ \mathbf{H}_{n1} & \cdots & \mathbf{H}_{nj} & \cdots & \mathbf{H}_{nn} \end{bmatrix}$$

Here the matrix block $\mathbf{H}_{ij} \in \mathbb{R}^{n_{\text{ao},i} \times n_{\text{ao},j}}$ and the choice of $n_{\text{ao},i}$ and $n_{\text{ao},j}$ atomic orbitals depend on the atoms i, j within their chemical environments. This fact underlies the construction of interaction modules in the models described in Section 5: they construct representations of atom pairs from representations of atomic environments.

Unfortunately, eigenvalues and wave function coefficients are not well-behaved or smooth functions because they depend on atomic coordinates and changing molecular configurations. This problem can be addressed by deep learning architectures that directly define the Hamiltonian matrix.

In this work, we propose a benchmark for both scalar parameter prediction, such as the conformation energy, and

prediction of matrix parameters such as the core Hamiltonian and overlap matrices.

4 Dataset

The first primary contribution of this work is a large-scale ∇ DFT dataset suitable for training expressive models for quantum chemical properties prediction. Our dataset is based on a subset of the Molecular Sets (MOSES) dataset.²⁷ The resulting dataset contains 1 004 918 molecules with atoms C, N, S, O, F, Cl, Br, and H. It contains 226 424 unique Bemis–Murcko scaffolds⁶¹ and 34 572 unique BRICS fragments.⁶²

For each molecule from the dataset, we have run the conformation generation method from the *RDKit* software^{63,64} suite proposed in Wang *et al.*⁶⁵ Next, we clustered the resulting conformations with the Butina clustering method,⁶⁶ finally taking the clusters that cover at least 95% conformations and using their centroids as the set of conformations. This procedure has resulted in 1 to 62 unique conformations for each molecule, with 5 340 152 total conformations in the full dataset. For each conformation, we have calculated its electronic properties including the energy (E), DFT Hamiltonian matrix (H), and DFT overlap matrix (S) (see the full list in Table 2). All properties were calculated using the Kohn–Sham method⁶⁷ at ω B97X-D/def2-SVP levels of theory using the quantum-chemical software package *Psi4*,⁶⁸ version 1.5. Default PSI4 parameters were used for DFT computations, *i.e.* Lebedev–Treutler grid with a Treutler partition of the atomic weights, 75 radial points and 302 spherical points, the criterion for the SCF cycle termination was the convergence of energy and density up to 10^{-6} threshold, integral calculation threshold was 10^{-12} .

We provide several splits of the dataset that can serve as the basis for comparison across different models. First, we fix the training set that consists of 100 000 molecules with 436 581 conformations and its smaller subsets with 10 000, 5000, and 2000 molecules and 38 364, 20 349, and 5768 conformations respectively; these subsets can help determine how much additional data helps various models. We choose another 100 000 random molecules as a structure test set. The scaffold test set has 100 000 molecules containing a Bemis–Murcko scaffold from a random subset of scaffolds which are not present in the training set. Finally, the conformation test set consists of 91 182 (resp., 10 000, 5000, 2000) molecules from the

training set with new conformations, numbering in total 92 821 (8892, 4897, 1724) conformations; this set can be used for the single-molecule setup.

As part of the benchmark, we provide separate databases for each subset and task and a complete archive with wave function files produced by the *Psi4* package that contains quantum chemical properties of the corresponding molecule and can be used in further computations.

A formal comparison of our dataset's parameters with previously available datasets such as QM9, ANI-1, and QMugs is presented in Table 1.

5 Methods

The goal of this benchmark is to advance and standardize studies in the field of machine learning methods for computational quantum chemistry. We focus on the class of models that predict quantum chemistry properties from the spatial representation of molecules. More precisely, we study models for two tasks:

- Conformational energy prediction and
- DFT Hamiltonian prediction

Fig. 2 shows a bird's eye overview of the general architecture for the models that we compare in this work. It consists of four main blocks:

- Inputs: all considered models use atom types, coordinates, or their functions as input.
- Embedding layers: MLP or a single linear layer.
- Interaction layers: this is usually the main part with model-specific architecture.
- Output layers: depending on the model, output layers are designed to convert internal representations into specific desired values.

5.1 Linear regression

We propose the linear regression model (LR) as a simple baseline for molecular properties prediction, in particular energy prediction. It takes the numbers of each atom type in the molecule as an input representation and predicts energy as its weighed sum. While it is clear that more sophisticated handcrafted features may increase a model's accuracy and generalization power, in this work we focus on deep models that can learn such features automatically.

Table 1 DFT dataset statistics

Statistic	QM9	ANI-1	QMugs	∇ DFT
Number of molecules	134k	57 462	665k	1m
Number of conformers	134k	20m	2m	5m
Number of atoms	3–29	2–26	4–228	8–62
Number of heavy atoms	1–9	1–8	4–100	8–27
Atomic species	H, C, N, O, F	H, C, N, O	H, C, N, O, P, S, Cl, F, Br, I	H, C, N, O, Cl, F, Br
Hamiltonian matrices	No	No	No ^a	Yes
Level of theory	B3LYP/6-31G(2df,p)+G4MP2	ω B97X/6-31G(d)	ω B97X-D/def2-SVP+GFN2-xTB	ω B97X-D/def2-SVP
Storage size	230 Mb	5.29 Gb	7 Tb	100 Tb

^a Hamiltonian matrices for QMugs dataset can be calculated from density matrices by one step of DFT cycle.

Table 2 Properties provided in DFT datasets

QM9	DFT + partially G4MP2: rotational constants, dipole moment, isotropic polarizability, HOMO/LUMO/gap energies, electronic spatial extent, zero point vibrational energy, internal energy at 0 K, internal energy at 298.15 K, enthalpy at 298.15 K, free energy at 298.15 K, heat capacity at 298.15 K, Mulliken charges, harmonic vibrational frequencies
ANI-1	DFT: total energy
QMugs	GFN2 + DFT: total, internal atomic and formation energies, dipole, rotational constants, HOMO/LUMO/gap energies, Mulliken partial charges GFN2: total enthalpy, total free energy, quadrupole, enthalpy, heat capacity, entropy, Fermi level, covalent coordination number, molecular dispersion coefficient, atomic dispersion coefficients, molecular polarizability, atomic polarizabilities, Wiberg bond orders, total Wiberg bond orders DFT: electrostatic potential, Löwdin partial charges, exchange correlation energy, nuclear repulsion energy, one-electron energy, two-electron energy, mayer bond orders, Wiberg-Löwdin bond orders, total mayer bond orders, total Wiberg-Löwdin bond orders, density/orbital matrices, atomic-orbital-to-symmetry-orbital transformer matrix
VDFT	DFT: electrostatic potential, Löwdin partial charges, exchange correlation energy, nuclear repulsion energy, one-electron energy, two-electron energy, mayer bond orders, Wiberg-Löwdin bond orders, total mayer bond orders, total Wiberg-Löwdin bond orders, density/orbital matrices, atomic-orbital-to-symmetry-orbital transformer matrix, Hamiltonian matrix

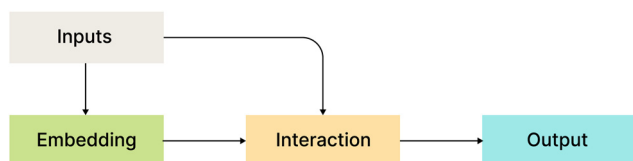


Fig. 2 High-level architecture of the models.

5.2 SchNet¹⁵

The *SchNet* model was one of the first works that suggested a neural architecture for atomic forces and molecular energy prediction. The key contribution here is the *cfconv*, a continuous-filter convolutional layer for modeling objects with arbitrary positions. The model is schematically represented in Fig. 3.

Given feature representations of n objects $X^l = (x_1, x_2, \dots, x_n) \in \mathbb{R}^F$, $X^l = (x_1, x_2, \dots, x_n) \in \mathbb{R}^F$ (at layer l), which are at positions $R = (r_1, \dots, r_n) \in \mathbb{R}^D$, and a special function W^l that maps R 's domain to X 's domain, *i.e.*, $W^l: \mathbb{R}^D \rightarrow \mathbb{R}^F$, the output of the proposed *cfconv* layer is defined as

$$x_i^{l+1} = (X^l \times W^l)_i = \sum_j x_j^l \circ W^l(r_i - r_j).$$

where \circ denotes element-wise multiplication.



Fig. 3 A schematic depiction of the *SchNet* architecture with its sub-units. The left column shows an overview, and middle and right columns detail the Interaction and *cfconv* blocks. X is an atom's representation, D_{ij} is the pairwise distance matrix. Atom-wise blocks are multilayer perceptrons applied to each atom representation independently.

The use of *cfconv* and the overall network architecture design ensure an important property: energy and force predictions are rotationally invariant and equivariant respectively. For instance, in the *cfconv* layer W^l is a combination of $\|r_i - r_j\|$, radial basis functions, dense feedforward layers, and a shifted *softplus* activation function $\text{sps}(x) = \ln(0.5e^x + 0.5)$.

The model takes nuclear charges and atomic positions as inputs. Nuclear charges are first embedded into 64-dimensional representations. After that, they are processed with an "Interaction" block of layers that includes 3 applications of *cfconv* (*cf.* Fig. 3, thus enriching the feature representation with positional information). Then more atom-wise modifications follow to be pooled in a final layer to obtain the energy prediction. Differentiating the energy with respect to atom positions yields the forces, hence force predictions can be and are also added to the loss function.

The resulting method has been tested on three datasets: QM9,^{37,69} MD17,⁷⁰ and ISO17 (introduced in the original work¹⁵). For more details we refer to Schutt *et al.*¹⁵

5.3 DimeNet⁷¹

A major contribution of *DimeNet* is that it takes into account not only the distances between pairs of atoms, but also angles formed by triples of atoms. The authors note that the pairwise distance matrix is sufficient to describe the full geometric information of the molecule. However, in order to keep computational costs reasonable graph neural networks (GNN) ignore connections between atoms that are more than a certain cutoff distance apart. One possible result of this simplification could be that the GNN would not be able to distinguish between some molecules.

DimeNet is inspired by the *PhysNet* model⁷² and expands it with message passing and additional directional information. A general overview of the architecture is shown in Fig. 4 (left). The core of *DimeNet* is the Interaction block: a message \mathbf{m}_{ji} from atom j to atom i takes into account information about the angles $\angle \mathbf{x}_i \mathbf{x}_j \mathbf{x}_k$ obtained *via* messages from the corresponding atoms k that are neighbors of atom j . Specifically, it is defined as follows:

$$\mathbf{m}_{ji}^{(l+1)} = f_{\text{update}} \left(\mathbf{m}_{ji}^{(l)}, \sum_{k \in \mathcal{N}_j \setminus \{i\}} f_{\text{int}} \left(\mathbf{m}_{kj}^{(l)}, \mathbf{e}_{\text{RBF}}, \mathbf{a}_{\text{SBF}}^{(kj,ji)} \right) \right),$$



Fig. 4 DimeNet++ architecture. Left to right: General structure, Embedding block, Output block.

where \mathcal{N}_j is the set of neighbors of atom j , $e_{\text{RBF}}^{(ij)}$ is the radial basis interatomic distance, and $\alpha_{\text{SBF}}^{(kj,ji)}$ is the directional information represented by spherical Bessel functions and spherical harmonics.

The Interaction block is visualized in Fig. 5. A message \mathbf{m}_{ji} is initialized with learnable embeddings $h_i^{(0)}$ and $h_j^{(0)}$ that depend on the relative position of corresponding atoms (Fig. 4, middle). Finally, the messages are combined together to form the atom embedding

$$\mathbf{h}_i = \sum_{j \in \mathcal{N}_i} \mathbf{m}_{ji},$$

which is further used to predict the energy (Fig. 4, right).

The resulting model is invariant to permutations, translation, rotation, and inversion. Evaluation on QM9 and MD17 shows that *DimeNet* significantly outperforms *SchNet* on the prediction of most targets. An extension of this model was later proposed in *DimeNet++*;⁷³ it further improved performance and reduced computational costs.

5.4 SchNorb¹⁶

This model is a direct continuation of the *SchNet* model¹⁵; the *SchNet* sub-architecture is used as a “first step” in the *SchNorb* model. The most important differences are the following: (1) *SchNorb* is designed to predict molecular energy, forces, the overlap matrix, and the Hamiltonian matrix; (2) directions (angles and normalized position differences) are used explicitly

to capture the interaction information and model various symmetries; (3) the loss function is a sum of errors in the prediction of energy, forces, Hamiltonian, and the overlap matrix (Fig. 6).

The inputs for this neural network are the charges Z and position differences $\|\mathbf{r}_{ij}\|$ (norm of the vector pointing from atom i to atom j); the model also uses normalized directions $\frac{\mathbf{r}_{ij}}{\|\mathbf{r}_{ij}\|}$. The representations Z and $\|\mathbf{r}_{ij}\|$ are then processed with the *SchNet* step as described in Section 5.2.

On the next *SchNorb* step, *SchNet* outputs (a vector per atom) are combined with $\|\mathbf{r}_{ij}\|$ using a factorised tensor layer,⁷⁴ feedforward layers, shifted softplus, and simple sums. The outputs include: (1) rotationally invariant per-atom embeddings \mathbf{X}^l , which are then transformed and aggregated to predict the energy value; (2) embeddings \mathbf{P}^l for atom pairs that are multiplied by different powers of directional cosines, aggregated and passed to fully connected layers to predict blocks of the Hamiltonian and overlap matrices; (3) finally, similar to *SchNet*, forces are predicted *via* graph differentiation.

The datasets used in this work are based on MD17⁷⁰ and include water, ethanol, malondialdehyde, and uracil. Reference calculations were performed with Hartree–Fock (HF) and density functional theory (DFT) with the PBE exchange correlation functional. For more details regarding data preparation and augmentation we refer to Schütt *et al.*¹⁶

5.5 SE3 (PhiSNet)

The *PhiSNet* model was suggested by Unke *et al.*¹⁷ The authors presented an SE(3)-equivariant architecture for predicting Hamiltonian matrices. The model improves over the results of *SchNorb* both in terms of equivariance (*SchNorb* is not SE(3)-equivariant, so its predictions for the same conformation in a different reference coordinate system may differ in unpredictable ways) and in terms of accuracy metrics for single compound datasets.

The main building blocks of *PhiSNet* are the following: (1) feature representation both for input and intermediate layers is of the form $\mathbb{R}^{F \times (L+1)^2}$, where F corresponds to feature channels and $(L+1)^2$ corresponds to all possible spherical harmonics of



Fig. 5 DimeNet++ architecture: the Interaction block.

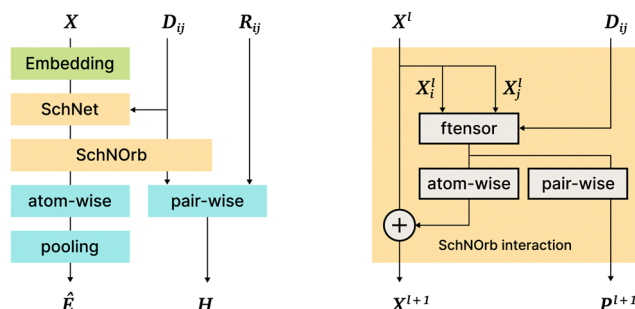


Fig. 6 The *SchNorb* architecture. On the left: general architecture overview; on the right: the *Interaction* block in *SchNorb*. In addition to the *SchNet Interaction* block, *SchNorb* uses the factorized tensor layer⁷⁴ to produce pairwise atom features and predict the basis coefficients for the Hamiltonian.

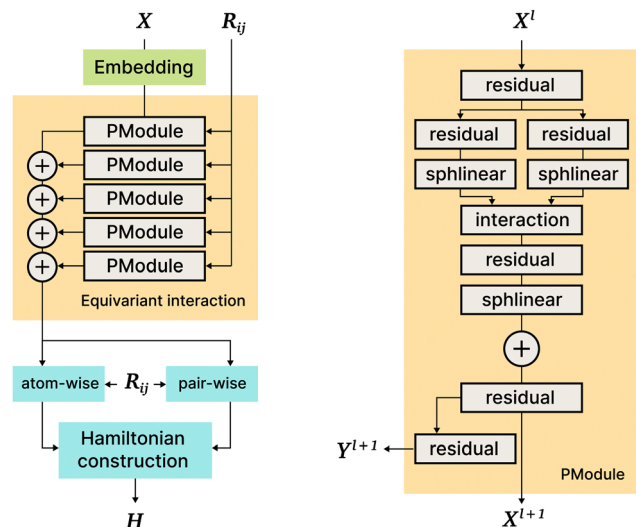


Fig. 7 *PhiSNet* architecture. On the left: General architecture overview; on the right: the *PModule* block in detail. More details about sphilinear and interaction blocks of *PModule* are given in phisnet2021.

degree $l \in \{0, \dots, L\}$; (2) all layers except the last one apply SE(3)-equivariant operations on features; matrix multiplication, tensor product contractions, and tensor product expansions are mixed together to make equivariant updates for the features of every atom and atom pair; on the last layer, the Hamiltonian and overlap matrices are constructed from pairwise features (Fig. 7).

We have made several minor modifications to the original model implementation of *PhiSNet* in order to allow it to work with the ∇ DFT dataset; in particular, we have applied batchization similar to *Pytorch Geometric*, where molecules inside a single batch are treated as one molecule with no bonds between atoms of different molecules.

6 Benchmark setup and results

We focus on two different tasks: DFT Hamiltonian matrix prediction and molecular conformation energy prediction. All models have been trained on 2k, 5k, 10k, and 100k subsets of ∇ DFT. For the first task we compare *SchNOrb* and *PhiSNet* models, while for the second task we compare linear regression, *SchNet*, *SchNOrb*, and *Dimenet++* models. In both tasks, our main goal is to measure the ability of state of the art models to generalize across a diverse set of molecules.

Metrics for energy prediction and prediction of Hamiltonian matrices are reported in Tables 3 and 4 respectively. These results lead us to the following observations.

First and foremost, we see that all models in both tasks, except *SchNOrb* and Linear Regression, benefit from increasing the dataset size. This indicates that even already published models may not have hit the limit of their expressive power and may further benefit from larger scale datasets. We suppose that linear model has almost identical scores trained on train sets of different sizes because of small expressiveness. Training has

Table 3 Energy prediction metrics: mean absolute error (MAE), less is better

Model	MAE for energy prediction, $\times 10^{-2} E_h$			
	2k	5k	10k	100k
Structure test split				
LR	4.6	4.7	4.7	4.7
<i>SchNet</i>	151.8	66.1	29.6	— ^a
<i>Dimenet++</i>	24.1	21.1	10.6	3.2
<i>SchNOrb</i>	5.9	3.7	13.3 ^a	— ^a
Scaffolds test split				
LR	4.6	4.7	4.7	4.7
<i>SchNet</i>	126.5	68.3	27.4	— ^a
<i>Dimenet++</i>	21.6	20.9	10.1	3.0
<i>SchNOrb</i>	5.9	3.4	14.8 ^a	— ^a
Conformations test split				
LR	4.0	4.2	4.0	4.0
<i>SchNet</i>	79.1	67.3	21.4	— ^a
<i>Dimenet++</i>	18.3	33.7	5.2	2.5
<i>SchNOrb</i>	5.0	3.6	14.5 ^a	— ^a

^a Training *SchNOrb* model did not converge for the 10k, and 100k train split, for *SchNet* model did not converge for the 100k train split.

Table 4 Prediction metrics for Hamiltonian and overlap matrices: mean absolute error, less is better

Model	MAE for Hamiltonian matrix prediction, $\times 10^{-3} E_h$			MAE for overlap matrix prediction, $\times 10^{-5}$		
	2k	5k	10k	2k	5k	10k
Structure test split						
<i>SchNOrb</i> ^a	386.5	383.4	382.0	1550	1571	3610
<i>PhiSNet</i>	7.4	3.2	2.9	5.1	4.3	3.5
Scaffolds test split						
<i>SchNOrb</i> ^a	385.3	380.7	383.6	1543	1561	3591
<i>PhiSNet</i>	7.2	3.2	2.9	5.0	4.3	3.5
Conformations test split						
<i>SchNOrb</i> ^a	385.0	384.8	392.0	1544	1596	3576
<i>PhiSNet</i>	6.5	3.2	2.8	5.1	4.6	3.6

^a While the relative difference between metrics for *SchNOrb* and *PhiSNet* is similar to the one reported by phisnet2021, we believe that there are still some problems with *SchNOrb* training in the multi-molecule setup, e.g., gradient explosion.

not converged in the case of *SchNOrb* model for 10k and 100k splits.

Second, as expected, the models perform better on the conformations test split that contains the same set of structures but with different conformations; in this case, the training set is most similar to the test set so this behaviour is expected. On the other hand, on the structures test split and the scaffolds test split the models show nearly equivalent performance. This may imply that models generalized on different structures automatically generalize on different scaffolds.

Third, interestingly, deep models that were trained on small dataset splits (2k, 5k, and 10k) only to predict energy show results worse than a simple linear regression. On the positive side, the *DimeNet++* model trained on the 100k subset performs

better, which may imply that the same model trained on the full training set may show much better results. Moreover SchNOrb models trained on 2k and 5k splits perform better than linear regression and other models trained on corresponding splits, which may imply that energy prediction benefits from multi-target (Hamiltonian matrix, overlap matrix and energy) learning.

Fourth, in our setup deep models for energy prediction perform much worse than they do on previously known benchmarks such as *QM9* or *MD17* (e.g. DimeNet++ has MAE $0.00023E_h$ on *QM9*⁷³). This may be caused by the diversity of the ∇ DFT dataset and small size of splits. The latter point holds for models for predicting Hamiltonian matrices as well; in this case, we see that as an indication that more care needs to be taken in hyperparameter tuning and construction of new architectures.

7 Conclusions

In this work, we present a unique molecular dataset containing results of DFT computations along with a number of deep neural network models designed to predict the computed properties. We have designed a number of different tests to assess the generalization capabilities of machine learning models across the chemistry domain, specifically the domain of medicinal chemistry. We have modified several publicly available neural network models to make them able to learn from conformations of multiple molecules instead of a single molecule. We share the code for modified models as well as their pretrained versions to simplify future research in this field.

Results of our experimental evaluation show the ability of modern deep neural networks to generalize, both for energy prediction and estimation of Hamiltonian matrices. We also see that increasing amount of data leads to better metrics, especially in the case of the *PhiSNet* model. Unfortunately, training with a limited amount of computational resources or small dataset size often leaves deep neural networks undertrained and exhibiting comparatively bad performance. In particular, model errors grow significantly in the multi-molecular setting compared to a single molecule. It still remains a challenge to obtain models that are superior to chemical accuracy.

Data and code accessibility

The code and links to the full dataset and its parts can be found at <https://github.com/AIRI-Institute/nablaDFT>.

Author contributions

Conceptualization: K. K., A. K. Methodology: K. K., S. N., A. K. Software: K. K., I. S., A. G., A. Ts., A. Tel., A. A. Validation: K. K., A. G. Investigation: K. K., I. S., A. Ts., A. Tel., A. A. Data curation: K. K. Writing – original draft: K. K., I. S., A. R., P. Z., S. N., A. K. Writing – review & editing: K. K., I. S., A. R., A. G., A. Ts., A. A., P. Z., S. N., A. K., P. S. Visualization: A.K. Supervision: A. K. Project administration: A.K.

Conflicts of interest

There are no conflicts to declare.

Acknowledgements

The work of S. N. was supported by a grant for research centers in the field of artificial intelligence, provided by the Analytical Center for the Government of the Russian Federation in accordance with the subsidy agreement (agreement identifier 000000D730321P5Q0002) and the agreement with the Ivannikov Institute for System Programming of the Russian Academy of Sciences dated November 2, 2021 No. 70-2021-00142.

Notes and references

- 1 R. J. Bartlett and J. F. Stanton, *Rev. Comput. Chem.*, 1994, 65–169.
- 2 B. L. Hammond, W. A. Lester and P. J. Reynolds, *Monte Carlo methods in ab initio quantum chemistry*, World Scientific, 1994, vol. 1.
- 3 P. Hohenberg and W. Kohn, *Phys. Rev.*, 1964, **136**, B864.
- 4 W. Kohn and L. J. Sham, *Phys. Rev.*, 1965, **140**, A1133.
- 5 R. M. Martin, *Electronic structure: basic theory and practical methods*, Cambridge university press, 2020.
- 6 A. Erba, J. Baima, I. Bush, R. Orlando and R. Dovesi, *J. Chem. Theory Comput.*, 2017, **13**, 5019–5027.
- 7 J. P. Perdew and Y. Wang, *Phys. Rev. B: Condens. Matter Mater. Phys.*, 1992, **45**, 13244.
- 8 J. P. Perdew, K. Burke and M. Ernzerhof, *Phys. Rev. Lett.*, 1996, **77**, 3865.
- 9 J. Tao, J. P. Perdew, V. N. Staroverov and G. E. Scuseria, *Phys. Rev. Lett.*, 2003, **91**, 146401.
- 10 C. Goringe, D. Bowler and E. Hernandez, *Rep. Prog. Phys.*, 1997, **60**, 1447.
- 11 C. W. Groth, M. Wimmer, A. R. Akhmerov and X. Waintal, *New J. Phys.*, 2014, **16**, 063065.
- 12 K. Choo, A. Mezzacapo and G. Carleo, *Nat. Commun.*, 2020, **11**, 1–7.
- 13 J. Hermann, Z. Schätzle and F. Noé, *Nat. Chem.*, 2020, **12**, 891–897.
- 14 G. Hegde and R. C. Bowen, *Sci. Rep.*, 2017, **7**, 1–11.
- 15 K. Schütt, P.-J. Kindermans, H. E. Sauceda Felix, S. Chmiela, A. Tkatchenko and K.-R. Müller, *Advances in neural information processing systems*, 2017, vol. 30, pp. 992–1002.
- 16 K. T. Schütt, M. Gastegger, A. Tkatchenko, K.-R. Müller and R. J. Maurer, *Nat. Commun.*, 2019, **10**, 1–10.
- 17 O. Unke, M. Bogojeski, M. Gastegger, M. Geiger, T. Smidt and K.-R. Müller, *Advances in Neural Information Processing Systems*, 2021, vol. 34, pp. 14434–14447.
- 18 H. Li, Z. Wang, N. Zou, M. Ye, W. Duan and Y. Xu, arXiv, 2021, preprint arXiv:2104.03786.
- 19 R. Nagai, R. Akashi, S. Sasaki and S. Tsuneyuki, *J. Chem. Phys.*, 2018, **148**, 241737.
- 20 R. Nagai, R. Akashi and O. Sugino, *npj Comput. Mater.*, 2020, **6**, 1–8.

- 21 X. Lei and A. J. Medford, *Phys. Rev. Mater.*, 2019, **3**, 063801.
- 22 P. Ramos and M. Pavanello, *arXiv*, 2019, preprint arXiv:1906.06661.
- 23 A. Ryabov, I. Akhatov and P. Zhilyaev, *Sci. Rep.*, 2020, **10**, 1–7.
- 24 L. Li, S. Hoyer, R. Pederson, R. Sun, E. D. Cubuk, P. Riley and K. Burke, *et al.*, *Phys. Rev. Lett.*, 2021, **126**, 036401.
- 25 J. Kirkpatrick, B. McMorro, D. H. Turban, A. L. Gaunt, J. S. Spencer, A. G. Matthews, A. Obika, L. Thiry, M. Fortunato and D. Pfau, *et al.*, *Science*, 2021, **374**, 1385–1389.
- 26 A. Ryabov, I. Akhatov and P. Zhilyaev, *Sci. Rep.*, 2022, **12**, 1–10.
- 27 D. Polykovskiy, A. Zhebrak, B. Sanchez-Lengeling, S. Golovanov, O. Tatanov, S. Belyaev, R. Kurbanov, A. Artamonov, V. Aladinskiy, M. Veselov, A. Kadurin, S. Johansson, H. Chen, S. Nikolenko, A. Aspuru-Guzik and A. Zhavoronkov, *Front. Pharmacol.*, 2020, **11**, 565644.
- 28 J. Irwin, T. Sterling, M. Mysinger, E. Bolstad and R. Coleman, *J. Chem. Inf. Model.*, 2012, **52**(7), 1757–1768.
- 29 L. Chanussot, A. Das, S. Goyal, T. Lavril, M. Shuaibi, M. Riviere, K. Tran, J. Heras-Domingo, C. Ho, W. Hu, A. Palizhati, A. Sriram, B. Wood, J. Yoon, D. Parikh, C. L. Zitnick and Z. Ulissi, *ACS Catal.*, 2021, **11**(10), 6059–6072.
- 30 R. Tran, J. Lan, M. Shuaibi, B. Wood, S. Goyal, A. Das, J. Heras-Domingo, A. Kolluru, A. Rizvi, N. Shoghi, A. Sriram, Z. Ulissi and C. L. Zitnick, *arXiv*, 2022, preprint arXiv:2206.08917.
- 31 A. Vaswani, N. Shazeer, N. Parmar, J. Uszkoreit, L. Jones, A. N. Gomez, L. U. Kaiser and I. Polosukhin, *Advances in Neural Information Processing Systems*, 2017.
- 32 J. Devlin, M.-W. Chang, K. Lee and K. Toutanova, Proceedings of the 2019 Conference of the North American Chapter of the Association for Computational Linguistics: Human Language Technologies, Volume 1 (Long and Short Papers), Minneapolis, Minnesota, 2019, pp. 4171–4186.
- 33 T. Brown, B. Mann, N. Ryder, M. Subbiah, J. D. Kaplan, P. Dhariwal, A. Neelakantan, P. Shyam, G. Sastry, A. Askell, S. Agarwal, A. Herbert-Voss, G. Krueger, T. Henighan, R. Child, A. Ramesh, D. Ziegler, J. Wu, C. Winter, C. Hesse, M. Chen, E. Sigler, M. Litwin, S. Gray, B. Chess, J. Clark, C. Berner, S. McCandlish, A. Radford, I. Sutskever and D. Amodei, *Advances in Neural Information Processing Systems*, 2020, pp.1877–1901.
- 34 Z. Miftahutdinov, A. Kadurin, R. Kudrin and E. Tutubalina, *Bioinformatics*, 2021, **37**, 3856–3864.
- 35 E. Tutubalina, A. Kadurin and Z. Miftahutdinov, Proceedings of the 28th International Conference on Computational Linguistics, 2020, pp. 6710–6716.
- 36 A. D. Becke, *J. Chem. Phys.*, 2014, **140**, 18A301.
- 37 L. Ruddigkeit, R. Van Deursen, L. C. Blum and J.-L. Reymond, *J. Chem. Inf. Model.*, 2012, **52**, 2864–2875.
- 38 J. S. Smith, O. Isayev and A. E. Roitberg, *Chem. Sci.*, 2017, **8**, 3192–3203.
- 39 J. S. Smith, O. Isayev and A. E. Roitberg, *Sci. Data*, 2017, **4**, 1–8.
- 40 T. Fink, H. Bruggesser and J.-L. Reymond, *Angew. Chem., Int. Ed.*, 2005, **44**, 1504–1508.
- 41 T. Fink and J.-L. Reymond, *J. Chem. Inf. Model.*, 2007, **47**, 342–353.
- 42 J.-D. Chai and M. Head-Gordon, *J. Chem. Phys.*, 2008, **128**, 084106.
- 43 D. Mendez, A. Gaulton, A. P. Bento, J. Chambers, M. De Veij, E. Félix, M. P. Magariños, J. F. Mosquera, P. Mutowo and M. Nowotka, *et al.*, *Nucleic Acids Res.*, 2019, **47**, D930–D940.
- 44 S. Grimme, C. Bannwarth and P. Shushkov, *J. Chem. Theory Comput.*, 2017, **13**, 1989–2009.
- 45 C. Bannwarth, S. Ehlert and S. Grimme, *J. Chem. Theory Comput.*, 2019, **15**, 1652–1671.
- 46 S. Grimme, *J. Chem. Theory Comput.*, 2019, **15**, 2847–2862.
- 47 J.-D. Chai and M. Head-Gordon, *Phys. Chem. Chem. Phys.*, 2008, **10**, 6615–6620.
- 48 F. Weigend and R. Ahlrichs, *Phys. Chem. Chem. Phys.*, 2005, **7**, 3297–3305.
- 49 J. C. Snyder, M. Rupp, K. Hansen, K.-R. Müller and K. Burke, *Phys. Rev. Lett.*, 2012, **108**, 253002.
- 50 J. Hermann, Z. Schätzle and F. Noé, *Nat. Chem.*, 2020, **12**, 891–897.
- 51 D. Pfau, J. S. Spencer, A. G. D. G. Matthews and W. M. C. Foulkes, *Phys. Rev. Res.*, 2020, **2**, 033429.
- 52 N. Gao and S. Günnemann, *arXiv preprint arXiv:2110.05064*, 2021.
- 53 R. A. Eremin, I. S. Humonen, P. N. Zolotarev, I. V. Medrish, L. E. Zhukov and S. A. Budenny, *Cryst. Growth Des.*, 2022, **22**, 4570–4581.
- 54 A. Yakubovich, A. Odinkov, S. I. Nikolenko, Y. Jung and H. Choi, *Front. Chem.*, 2021, **9**, 800133.
- 55 X. Wan, Z. Zhang, W. Yu and Y. Guo, *Materials Reports: Energy*, 2021, **1**, 100046.
- 56 G. R. Schleder, C. M. Acosta and A. Fazzio, *ACS Appl. Mater. Interfaces*, 2020, **12**, 20149–20157.
- 57 C. L. Ritt, M. Liu, T. A. Pham, R. Epszstein, H. J. Kulik and M. Elimelech, *Sci. Adv.*, 2022, **8**, eabl5771.
- 58 J. P. Janet, C. Duan, A. Nandy, F. Liu and H. J. Kulik, *Acc. Chem. Res.*, 2021, **54**, 532–545.
- 59 N. Ye, Z. Yang and Y. Liu, *Drug Discovery Today*, 2022, **27**, 1411–1419.
- 60 R. A. Mata and M. A. Suhm, *Angew. Chem., Int. Ed.*, 2017, **56**, 11011–11018.
- 61 G. W. Bemis and M. A. Murcko, *J. Med. Chem.*, 1996, **39**, 2887–2893.
- 62 J. Degen, C. Wegscheid-Gerlach, A. Zaliani and M. Rarey, *ChemMedChem*, 2008, **3**, 1503–1507.
- 63 RDKit: Open-source cheminformatics, <https://www.rdkit.org>.
- 64 G. Landrum, P. Tosco, B. Kelley, Ric, sriniker, gedeck, R. Vianello, NadineSchneider, E. Kawashima, A. Dalke, D. N, D. Cosgrove, B. Cole, M. Swain, S. Turk, Alexander-Savelyev, G. Jones, A. Vaucher, M. Wójcikowski, I. Take, D. Probst, K. Ujihara, V. F. Scalfani, guillaume godin, A. Pahl, F. Berenger, JLVarjo, strets123, JP and DoliathGavid, rd-kit/rdkit: 2022_03_1 (Q1 2022) Release, 2022, DOI: [10.5281/zenodo.6388425](https://doi.org/10.5281/zenodo.6388425).

- 65 S. Wang, J. Witek, G. A. Landrum and S. Riniker, *J. Chem. Inf. Model.*, 2020, **60**, 2044–2058.
- 66 J. M. Barnard and G. M. Downs, *J. Chem. Inf. Comput. Sci.*, 1992, **32**, 644–649.
- 67 L. J. Sham and W. Kohn, *Phys. Rev.*, 1966, **145**, 561.
- 68 D. G. Smith, L. A. Burns, A. C. Simmonett, R. M. Parrish, M. C. Schieber, R. Galvelis, P. Kraus, H. Kruse, R. Di Remigio and A. Alenaizan, *et al.*, *J. Chem. Phys.*, 2020, **152**, 184108.
- 69 R. Ramakrishnan, P. O. Dral, M. Rupp and O. A. Von Lilienfeld, *Sci. Data*, 2014, **1**, 1–7.
- 70 S. Chmiela, A. Tkatchenko, H. E. Sauceda, I. Poltavsky, K. T. Schütt and K.-R. Müller, *Sci. Adv.*, 2017, **3**, e1603015.
- 71 J. Gasteiger, C. Yeshwanth and S. Günnemann, *Advances in Neural Information Processing Systems*, 2021, pp. 15421–15433.
- 72 O. T. Unke and M. Meuwly, *J. Chem. Theory Comput.*, 2019, **15**, 3678–3693.
- 73 J. Gasteiger, S. Giri, J. T. Margraf and S. Günnemann, *Machine Learning for Molecules Workshop*, NeurIPS, 2020.
- 74 K. T. Schütt, F. Arbabzadah, S. Chmiela, K. R. Müller and A. Tkatchenko, *Nat. Commun.*, 2017, **8**, 1–8.